Sustainable Energy & Fuels

ROYAL SOCIETY OF CHEMISTRY

COMMUNICATION

View Article Online
View Journal | View Issue

Cite this: *Sustainable Energy Fuels*, 2026, **10**, 1408

Received 1st December 2025
Accepted 9th February 2026

DOI: 10.1039/d5se01588j

rsc.li/sustainable-energy

A porphyrin polyethylenimine polymer as an effective photosensitiser for hydrogen evolution

Patrick Loftus, Leila Tabrizi, Michael P. Brandon and Mary T. Pryce *

Photocatalytic hydrogen evolution is a promising approach to generate hydrogen gas for use as a green alternative to fossil fuels which have contributed to climate change. Simple metal oxide semiconductors have been studied extensively in photocatalysis, however these systems are limited by their broad band gap energy. Herein, the synthesis of and photophysical characterisation of a zinc tetraphenyl porphyrin appended branched polyethylenimine polymer (PEI-ZnTPP) is reported. The photophysical porperties of the PEI-ZnTPP polymer are similar to porphyrins in the literature, with an absorption profile that extends into the visible region of the electromagnetic (EM) spectrum, and a long lived triplet excited state lifetime of 197 μs. These visible light absorption properties were exploited using the polymeric nature of the PEI-ZnTPP to prepare PEI-ZnTPP/TiO_2/Pt^0 nanocomposites which displayed a photocatalytic hydrogen evolution rate of 34 675 μmol g^{-1} h^{-1} thus out-performing other photosensitising polymers coated onto TiO_2 in the literature. X-ray photoelectron spectroscopy of the nanocomposites indicated all components required for photocatalysis remained in the system following irradiation and were still available to act as PHE components, however slight degration of the coatings occurred. Using electrochemical analysis, a Rehm–Weller type thermodynamic analysis was performed for the nanocomposites indicating favourable electron transfer from the PEI-ZnTPP polymer to the TiO_2 and the Pt^0 co-catalyst, helping to further rationalise the impressive PHE rate observed for the nanocomposites.

Introduction

Climate change is one of the most pressing issues we face which is exacerbated by the release of CO_2 from fossil fuels into the atmosphere.[1] CO_2 concentrations in the atmosphere in 2023 were the highest in the past 800 000 years, and 2024 was the warmest year on record in the last 175 years.[2] Hydrogen gas is a potential candidate as an alternative energy carrier, releasing only H_2O as a by-product upon combustion.[3] However, the majority of hydrogen produced globally is fossil fuel derived, produced *via* the process of steam-methane reforming.[4] However, photocatalytic water splitting presents itself as a potential green route to H_2 production.[5]

In 1972, Fujishima and Honda first reported the use of TiO_2 to photoelectrochemically reduce water to hydrogen gas in the presence of a platinum electrode.[6] However, TiO_2 has a broad band gap (3.0–3.2 eV) hence it can only absorb high energy light in the UV region of the EM spectrum.[7] UV irradiation only contributes to a total of 4% of all solar irradiation, hence TiO_2 is restricted in its photocatalytic hydrogen evolution (PHE) efficiency.[8]

Porphyrins are a group of photosensitisers (PS) that consist of a tetrapyrrolic macrocyclic ring joined *via* methine bridges, resulting in the formation of an 18π aromatic ring.[9] The π electrons in this ring readily absorb light in the visible region of the EM spectrum, undergoing π–π* transitions as described by Gouterman's four orbital model.[10] This broad absorbance coupled with good photostability, and fluorescence properties has resulted in the use of porphyrins in a wide range of applications, including photocatalysis, photodynamic therapy, and bioimaging.[11–14] Recently there have been many examples where porphyrins have been used in conjunction with TiO_2 as heterogeneous PHE systems.[15–19] Many of these attempts have been proven to be very effective, for example Nikolaou *et al.* reported chemisorption of a porphyrin–boron dipyrromethene (BODIPY) assembly onto TiO_2, achieving an impressive PHE rate of 225 000 μmol H_2 g^{-1} h^{-1}.[20] In a separate report by Nikolaou *et al.* the use of platinum metalated porphyrins bearing carboxylic acids were used to simultaneously act as photosensitisers (PS) and catalysts when chemisorbed on the surface of Pt–TiO_2 nanoparticles, achieving a PHE rate of 707 000 μmol H_2 g^{-1} h^{-1}.[21] These heterogeneous approaches rely upon injection of electrons from the PS into the conduction band of the TiO_2 semiconductor facilitating their transfer to the Pt^0 co-catalyst, compared to homogeneous systems which rely upon intermolecular collisions between PS and catalyst for electron transfer.[15] Combining porphyrin photosensitising

School of Chemical Sciences, Dublin City University, Glasnevin, Dublin, D09 V289, Ireland. E-mail: mary.pryce@dcu.ie

units with the TiO_2 semiconductor extends the electronic absorption spectrum from the UV region of the EM spectrum to the visible region. Additionally charge separation *via* injection of electrons from the porphyrin units to the TiO_2 semiconductor helps to inhibit charge recombination and thus increases the efficiency of the PHE system.

Herein, the synthesis of a branched polyethylenimine polymer appended with zinc tetraphenyl porphyrin units (PEI-ZnTPP) is reported (Fig. 1). The photophysical properties and excited state dynamics of the PEI-ZnTPP polymer are described. The polymeric nature of the PEI-ZnTPP was used to coat TiO_2 yielding PEI-ZnTPP/TiO_2/Pt^0 nanocomposites, which were used to efficiently fuel heterogenous PHE. In order to understand this promising PHE rate, X-ray photoelectron spectroscopy (XPS) analysis of the nanocomposites was performed to assess their stability under photocatalytic conditions, and cyclic voltammetry (CV) was used to prepare a Rehm–Weller type thermodynamic analysis of the thermodynamic feasibility of electron transfer from the PEI-ZnTPP polymer to the TiO_2 semiconductor surface and hydrogen evolving Pt^0 co-catalyst.

Results and discussion

Synthesis and characterisation

Zinc(II) 4-(10,15,20-triphenylporphyrin-5-yl)benzoic acid, Zn(II) (Zn-COOH-TPP) was used as the porphyrin for covalent attachment to the polyethylenimine back bone (PEI). Zn-COOH-TPP was achieved through the preparation of methyl mono(-pcarboxy)tetraphenylporphyrin (Me-pcTPP) using the Lindsey method, using a one-pot two-step reaction of pyrrole, benzaldehyde and methyl-4-formylbenzoate under $BF_3 \cdot OEt_2$ catalysis followed by oxidation using 2,3-dichloro-5,6-dicyano-1,4-benzoquinone (DDQ). As reported by Lindsey *et al.* , a 0.1 M NaCl solution in CH_2Cl_2 was employed, as the reaction medium to improve the yield of Me-pcTPP.[22] Zinc was then coordinated to the porphyrin core by treating Me-pcTPP with zinc acetate hexahydrate in CH_2Cl_2/MeOH (7 : 3) under reflux. Hydrolysis of the methyl ester group was achieved by treatment with LiOH in THF/H_2O (4 : 1) mixture. Following an acidic work up with citric acid, the desired Zn-COOH-TPP was obtained (the reaction pathway for the preparation of Zn-COOH-TPP is given in Scheme S1). The PEI-ZnTPP polymer (Fig. 1) was prepared by the condensation reaction of Zn-COOH-TPP with oxalyl chloride followed by coupling to commercially available branched polyethylenimine (Scheme S2).

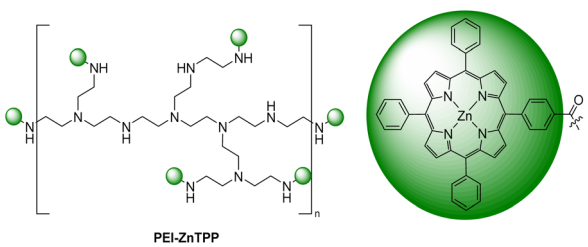

Fig. 1 Structure of PEI-ZnTPP.

Successful synthesis of the PEI-ZnTPP polymer was confirmed using ^{1}H NMR spectroscopy and FT-IR spectroscopy (Fig. S7–S11). On comparison of the ^{1}H NMR spectra of the PEI-ZnTPP with that of PEI (Fig. S8), new peaks (7.7–9.18 ppm) assigned to porphyrin protons were observed. The relative intensity of the peaks (0.25–3.40 ppm) were attributed to the –CH_2– protons of the PEI polymer back bone. The structure of the PEI-ZnTPP polymer was further confirmed by the FT-IR spectra. The intensity of the stretching vibrations of the N–H of the amino groups at 3588 cm^{-1} disappeared in the FT-IR spectrum of PEI-Zn TPP polymer (Fig. S10 and S11). Meanwhile, a new peak ~1700 cm^{-1} was assigned to C=O stretching vibrations of the amides in PEI-Zn TPP polymer, compare with free polymer PEI.

Gel permeation chromatography (GPC) analysis of PEI-ZnTPP shows a number-average molecular weight (M_n) of 6900 g mol^{-1} and a weight-average molecular weight (M_w) of 7164 g mol^{-1}, with a very narrow dispersity ($Đ$ = 1.04), indicating a well-defined and uniform polymer structure (Fig. S12 and Table S1). Consistently, the ESI-MS spectrum (Fig. S13) displays a dominant signal centred at m/z 7105.28, which is in good agreement with the molecular weight obtained from GPC. The close correspondence between the mass spectrometric data and GPC results confirms the successful formation of PEI-ZnTPP with controlled molecular weight and low polydispersity. The PEI polymer used was commercially available from Sigma-Aldrich with an average Mn ~600 g mol^{-1} by GPC.

Absorption and emission properties of PEI-ZnTPP

Steady state absorption and emission spectra for PEI-ZnTPP were recorded both in toluene and tetrahydrofuran (THF) (Fig. 2, S15, and Table S2). The UV-vis absorption spectrum consists of an intense absorption band at 424 nm corresponding to the Soret-Band absorption, which is typical of porphyrin macrocycles. This absorption band arises from the π–π* transition of electrons in the 18π aromatic system of the porphyrin ring from the ground state (S_0) to the second excited state (S_2). Two further, less intense absorption bands occur at 549 nm and 589 nm arising from the forbidden Q (0, 0) and Q (0, 1) transitions, respectively. These bands arise from excitation from S_0 to the first excited state (S_1). No significant shifts in wavelength or profile were evident compared to ZnTPP.[23] Additionally no significant peak broadening is apparent, with the full width half maximum (FWHM) of the Soret-Band of PEI-ZnTPP being

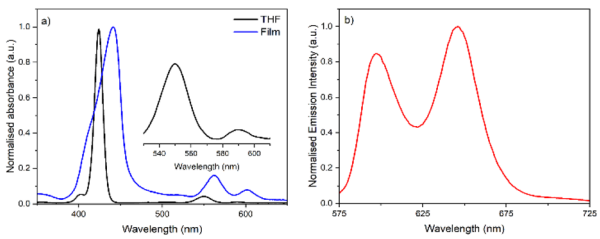

Fig. 2 (a) Absorption spectrum of PEI-ZnTPP in THF and a 0.1 mg film deposited on glass, insert; expansion of Q-bands (b) emission spectrum of PEI-ZnTPP in THF, λ_{ex} 425 nm.

650 cm^{-1}, only a difference of 23 cm^{-1} compared to the FWHM reported by Rochford *et al.* for ZnTPP in toluene. The absence of any shift in absorbance wavelength of the Soret-band is indicative of no aggregation for the polymeric porphyrin, as is frequently observed in the literature.[24,25] When the absorption spectra of thin films of PEI-ZnTPP are compared to those in solution (Fig. 2) a redshift of 18 nm was observed for the Soret band, together with an increase in the FWHM to 1878 cm^{-1}. These spectral changes are indicative that aggregation occurs for PEI-ZnTPP in the solid state.[26]

The PEI-ZnTPP polymer displayed emission maxima at 600, and 656 nm as a result of relaxation of the Q (0,0) and Q(0,1) transitions, respectively (Fig. 2). The Stokes' shift of the Q (0,0) transition was calculated to be 311 cm^{-1} for PEI-ZnTPP, representing an increase of 141 cm^{-1} compared to the stokes shift of 170 cm^{-1} reported for ZnTPP in toluene.[27] A fluorescence lifetime of 2 ns and quantum yield of 3% was obtained (Fig. S18 and S19). This short lifetime, coupled with the low fluorescence quantum yield is typical of porphyrins which readily undergo ISC populating the triplet excited state.[28] Evidence for population of the triplet excited state was confirmed *via* low-temperature (77 K) phosphorescence spectra of PEI-ZnTPP in a diethyl ether/ethanol/toluene solvent glass (Fig. S17). An emission band centred at 782 nm was observed, which is consistent with phosphorescence from the triplet excited state reported in the literature for tetraphenyl porphyrins.[29,30] In general, PEI-ZnTPP maintains the steady state absorption and emission properties of the ZnTPP PS units post binding to the polymer backbone. Hence, PEI-ZnTPP has the potential for solar energy harvesting and ultimately for PHE at the Pt^0 catalytic sites.

Triplet excited state properties of PEI-ZnTPP

Transient absorption spectroscopy (TAS) (Fig. 3, S20 and S21) was carried out using 355 nm excitation. In the TAS maps ground state bleaches (GSB) are evident in the ranges 543–572 nm and 592–602 nm which correspond to the Q band absorptions. The formation of new excited state absorption (ESA) features are evident between 435–543 nm, and 572–592 nm, attributed to the population of the $^3(\pi-\pi^*)$ excited state. The signals associated with the formation of the triplet excited state had a biexponential decay with two lifetime components of 28 and 123 μs (THF) (29 and 146 μs in toluene). The observation is consistent with the literature for other polymeric systems and is attributed to folding of the polymeric backbone which results in the formation of different microenvironments.[31,32] Different PS units are exposed to external factors (*e.g.* solvent) to varying degrees, and thus the decay pathways, in their respective microenvironment may vary, thereby resulting in the observation of a multicomponent excited state lifetime. However, when TAS studies were performed at lower concentrations, where folding of the polymer is less likely, monoexponential decays with lifetimes of 197 μs (toluene), 200 μs (THF) were obtained. Additionally a 211 μs lifetime was observed in the presence of the ascorbic acid sacrificial electron donor used during photocatalysis (Fig. S22). These lifetimes are similar to those reported by Bozdemir *et al.* (190 μs) for ZnTPP.[33] It should be noted that, as mentioned previously, there was no apparent evidence for aggregation of the polymer in the absorption spectra. However Parra *et al.* have reported that aggregation of porphyrin units results in a decrease in triplet excited state lifetime, and in the case of *meso*-tetrakis (4-sulfonatophenyl) porphyrin from 160 μs to 90 μs following aggregation.[34] Hence, it should also be considered that the additional, shorter lifetime component observed in the ns-TAS of PEI-ZnTPP at higher concentrations may be as a result aggregation.

The singlet oxygen quantum yield (Φ_Δ) was obtained for PEI-ZnTPP *via* phosphorescence at 1270 nm, using ZnTPP (Φ_Δ = 0.70) as a reference.[33] For PEI-ZnTPP, $\Phi_\Delta = 0.68$, which is largely unchanged from ZnTPP indicating that attachment of the ZnTPP units to the PEI backbone had no significant influence on the photophysical properties of the ZnTPP units incorporated onto the polymer backbone. These measurements indicate a quantum yield of more than 70% for the triplet state, which is beneficial for hydrogen generation.

Singlet oxygen is a strong oxidant, which may result in degradation of the various functionalities of the PEI-ZnTPP polymer.[35] Thus, in order to assess the stability of the PEI-

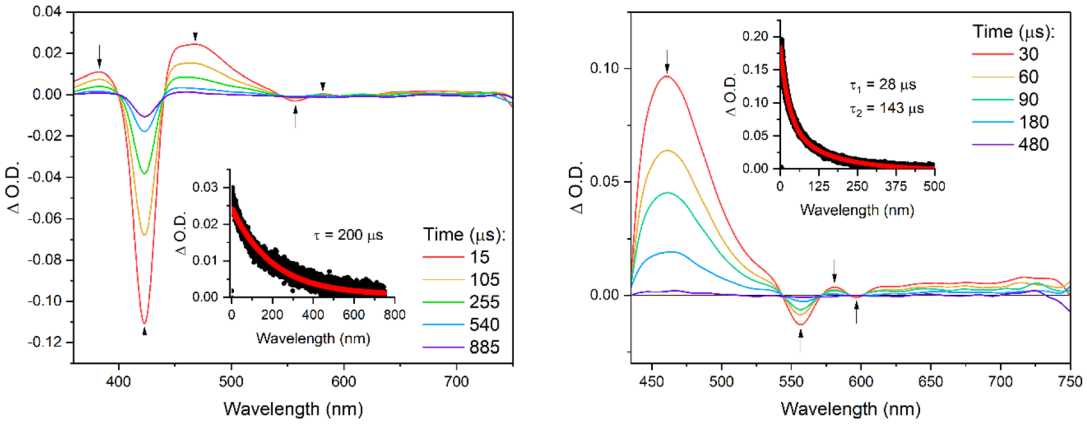

Fig. 3 ns-transient absorption maps of PEI-ZnTPP recorded in THF using a 355 nm excitation probe left) sample absorbance 0.01 a.u. at probe wavelength, right) sample absorbance 0.3 a.u. at probe wavelength. Insert: kinetic trace for ESA feature.

ZnTPP to the singlet oxygen generated *in situ*, samples of the PEI-ZnTPP were irradiated, and changes in the UV spectra were recorded (Fig. S14). Following 4 hours irradiation, no apparent bleaching of the Soret-band of the PEI-ZnTPP were observed, this indicating no degradation of the porphyrin units on this timescale. This potential degradation is also expected to be minimised under photocatalytic conditions given the deaeration of the samples prior to photocatalytic experiments.

Photocatalytic hydrogen evolution

The PEI-ZnTPP polymer was assessed as a light harvester for photocatalytic hydrogen evolution when coated on TiO_2 in the presence of 1 wt% Pt^0 and ascorbic acid as the sacrificial electron donor (SED). Photocatalytic experiments using aqueous 20% v/v triethanolamine (pH 7, adjusted with HCl) and 20% v/v methanol SED solutions resulted in only trace amounts of H_2 being evolved from the system. All experiments were conducted using a solar simulator (λ_{exc} 400–900 nm), ensuring visible light irradiation of the PEI-ZnTPP polymer, and minimizing direct excitation of the TiO_2 *via* UV irradiation.

Initially a series of different PEI-ZnTPP coatings on 5 mg of TiO_2 (0.1 mg, 0.2 mg, 0.4 mg, 0.8 mg, 1.2 mg) were assessed for PHE activity following 4 hours irradiation (Fig. 4). The higher loadings of PEI-ZnTPP onto TiO_2 resulted in lower PHE rates, with the 0.1 mg loading having the highest PHE rate of 34 675 μmol H_2 g^{-1} h^{-1} after 4 hours, compared to the 1.2 mg loading which only resulted in 5300 μmol H_2 g^{-1} h^{-1}. This decrease in activity at higher loadings is consistent with other reports in the literature, attributing this to agglomeration of material at the semiconductor surface resulting in ineffective penetration of incident photons through the agglomerated material and thus inhibition of electron flow to the metal co-catalyst diminishing PHE activity. Suryani *et al.* reported larger loadings of a dibenzo-BODIPY-phenothiazine based PS on TiO_2 agglomerating at the TiO_2 surface lowering PHE rates.[36] In a similar report, Mukherjee *et al.* reported the synthesis of a porous porphyrin polymer, which was used for PHE *via* mechanochemical incorporation of TiO_2 into the polymer, and *in situ* photodepostion of Pt^0. At higher TiO_2 content, agglomeration occurred which reduced the rate of PHE.[37]

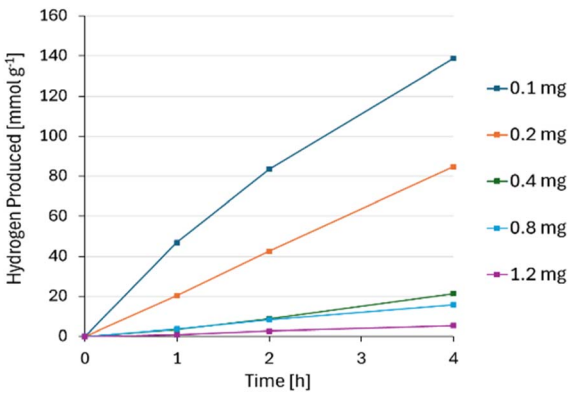

Fig. 4 Difference in PHE rate using different loadings of PEI-ZnTPP on TiO_2.

Control experiments were performed to verify that all components (PEI-ZnTPP/TiO_2/Pt^0 nanocomposite) were required for PHE (Table S5). In the absence of light, SED or co-catalyst, no hydrogen was detected. When PEI-ZnTPP is omitted from the experiments, hydrogen evolution did occur but was substantially less at 16 μmol of H_2 observed after 24 hours. The production of hydrogen is attributed to the anatase TiO_2 that was used, which has an absorption edge that tails to 400 nm.[38] However, in the presence of PEI-ZnTPP there was a fourfold increase with 59 μmol H_2 produced after 24 h (24 600 μmol g^{-1} h^{-1}). The activity of PEI-ZnTPP was also compared to ZnTPP to verify that the introduction of the polymeric backbone within the PS had a role in the observed increase. Following irradiation of the ZnTPP/TiO_2/Pt^0 nanocomposite for 24 h, 20 μmol of hydrogen was measured. As both PEI-ZnTPP and ZnTPP display similar photophysical properties, the PEI-ZnTPP containing nanocomposites are more effective at PHE relative to those prepared using ZnTPP. Reports in the literature have shown that TPP requires the presence of anchoring groups for efficient interaction with TiO_2.[39] As the PS units of PEI-ZnTPP also lack anchoring groups the increase in observed PHE activity is attributed to the PEI polymer backbone. Liu *et al.* have shown that a photosensitising polyaniline polymer adsorbed onto a TiO_2/Pt^0 surface *via* hydrogen bonding interactions, generates hydrogen (61.8 μmol g^{-1} h^{-1}).[40] The PEI backbone in PEI-ZnTPP is amine rich, and is reported to undergo hydrogen bonding interactions with TiO_2 under acidic conditions.[41] Thus, in this study, it is proposed that under PHE conditions the amine groups present in the PEI-ZnTPP polymer backbone also undergo hydrogen bonding with TiO_2, thereby allowing for electron injection from the excited PS units into the TiO_2 conduction band fuelling photocatalysis. Based on the above results, the combination of both the effective light harvesting ability of the ZnTPP units and the PEI backbone plays a role in both surface immobilisation of the photosensitiser in these nanocomposites and in harnessing light in the visible region of the EM spectrum for effective photocatalysis.

The activity of the composite of PEI-ZnTPP/TiO_2/Pt^0 relative to other composites in the literature incorporating a photosensitising polymer on TiO_2, is one of the most effective combinations reported to date (Table 1).[42–47] PEI-ZnTPP outperforms systems reported using pyrrole-based BODIPY PSs including the BODIPY-thiophene covalent organic polymer

Table 1 Comparison of PHE activity of polymer sensitised TiO_2 based photocatalytic systems reported in the literature

Compound	Co-Cat	SED	HER[a]	Ref.
PEI-ZnTPP	Pt^0	AA	34 675	This work
BODIPY-TH-COP1-OH_TiO_2	None	MeOH	197	43
HPCB	Pt^0	TEOA	3122	44
PDPP[T]$_2${TEG}-Flu-3	None	EtOH	8.06[b]	45
TSO_2@TiO_2	None	AA	11 220	46
UN-IEP-7@T-10	None	MeOH	3100	47
TT-Ant	Pt^0	MeOH	700	48

[a] μmol g^{-1} h^{-1}. [b] μmol h^{-1}.

reported by Turgut *et al.* with a PHE rate of 197 μmol g^{-1} h^{-1}, and the BODIPY based conjugated porous polymer (UN-IEP-7@T-10) reported by Palenzuela-Rebella *et al.* with a PHE rate of 3100 μmol g^{-1} h^{-1}.[42,46] PEI-ZnTPP also outperformed the hyper-branched poly (curcumin-1,3-bis (bromomethylbenzene) polymer reported by Mao *et al.* which was also used in conjunction with a Pt^0 co-catalyst.[43] From our studies the PEI-ZnTPP sensitised Pt^0/TiO_2 nanocomposites are effective at the harvesting of visible light and the transfer of excited state electrons to the Pt^0 co-catalyst *via* TiO_2.

Many recently reported heterogeneous PHE systems are designed in the absence of metal oxide semiconductors such as TiO_2, relying instead on direct injection of electrons to Pt^0 catalysts directly deposited on photoactive materials. Some of these systems have been proven to be quite effective such at the Pt porphyrin-fluorene based (PPF-Pt-Br) conjugated poly-electrolyte reported by Zhao *et al.* which achieved a PHE rate of 37 900 μmol H_2 g^{-1} h^{-1}.[48] However, many of these systems where Pt^0 co-catalysts are directly loaded onto supramolecular porphyrin structures fail to meet the PHE activity of the PEI-ZnTPP/TiO_2/Pt^0 nanocomposites herein reported. Chen *et al.* reported an ethynyl bridged ZnTPP/CoTPP (Zn-CoDETPP) conjugated polymer with a PHE rate of 43 μmol g^{-1} h^{-1}, Xu *et al.* reported a tetraphenylethylene-porphyrin covalent organic framework (COF) with a PHE rate of 58.4 μmol g^{-1} h^{-1}, Chen *et al.* reported a ZnTPP-2,5-diethoxyterephthalohydrazide COF with a PHE rate of 413 μmol g^{-1} h^{-1}, and Lv *et al.* reported a ZnTPP-thieno[3,2-*b*]thiophene-2,5-dicarbaldehyde COF (Zn-Por-TT-COF) with a PHE rate of 8200 μmol g^{-1} h^{-1}.[49–52] Despite all of the aforementioned examples having Pt^0 directly photodeposited onto their highly conjugated porphyrin structures, they did not display PHE rates as high as the PEI-ZnTPP/TiO_2/Pt^0 nanocomposites exhibited, further highlighting the benefit conferred upon the reported system as a result of the electron transport properties afforded by the TiO_2 semiconductor at the core of the nanocomposites.

X-ray photoelectron spectroscopy

X-Ray photoelectron spectroscopy was recorded on samples of the PEI-ZnTPP/TiO_2/Pt^0 nanocomposites before and after 4 h irradiation under PHE conditions (Fig. 5) to assess the stability of the nanocomposites. Two peaks are present in the Ti 2p spectra of the nanocomposites before and after irradiation with binding energies of 458.6 (Ti $2p_{3/2}$) and 465 (Ti $2p_{1/2}$) eV. These binding energies are consistent with Ti^{4+}, as is expected given the presence of the TiO_2 in the PHE system.[53] There are no observable shifts in binding energy or profile of the Ti^{4+} species before and after irradiation, indicating that there is no chemical changes to the TiO_2 post photocatalysis.

In the Pt 4f XPS spectra before photocatalysis there are two main peaks with binding energies of 70.6 and 74.4 eV, consistent with the XPS spectra reported for metallic platinum (Pt^0) confirming deposition of the Pt^0 catalytic centres.[54] There is evidence of Pt^{2+} present, based on the two peaks with binding energies at 72.8 and 76.1 eV.[55] Pt^{2+} most likely forms as the result of the deposition of Pt oxide species on the TiO_2 which have been

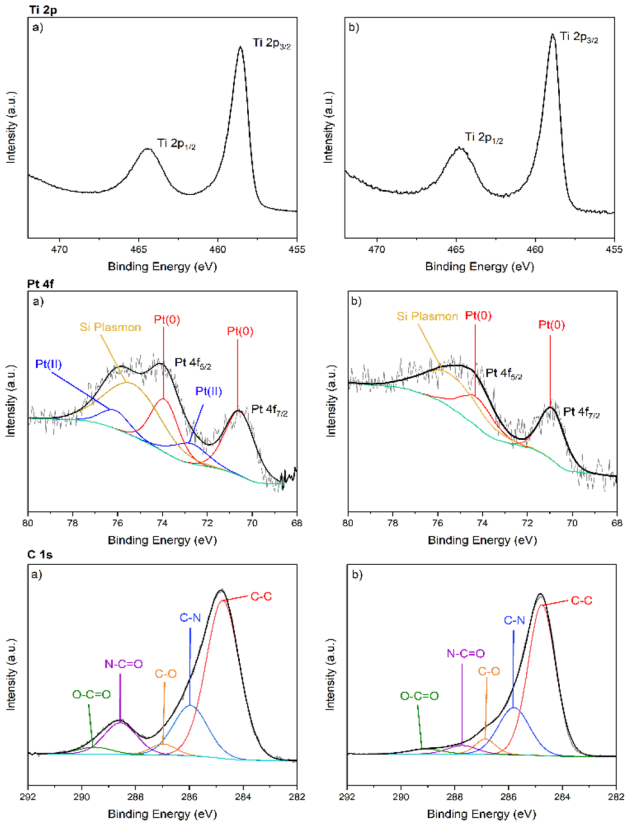

Fig. 5 XPS spectra of PEI-ZnTPP/TiO_2/Pt^0 nanocomposites (a) prior and (b) post 4 hours irradiation under photocatalytic conditions, note; in the Pt 4f spectra Si Plasmons have been assigned, as a result of a silicon grease impurity present in the taps of the Schlenk vessels uses to prepare samples for PHE.

reported by other groups to form early during the Pt photodeposition prior to complete conversion to Pt^0.[54] Following irradiation the two peaks assigned to Pt^0 remain, thus indicating that Pt^0 remains deposited on the TiO_2 surface, and furthermore there is no evidence that additional Pt^{2+} forms during the photocatalysis experiments. However, XPS analysis does indicate that that the loading of the Pt^0 deposits decreased from 0.2% in the pristine sample to 0.1% following irradiation, but the nanocomposites remained active over the 4 h experiment period.

Prior to irradiation three main peaks are observed in the C 1s XPS spectrum with binding energies of 284.8, 286.0, and 288.6 eV. The peak at 284.8 eV is assigned to C–C centres of the PEI backbone. The C–N environments associated with the amide linkage and terminal amines of the PEI backbone have been assigned at 286.0 eV, and the peak at 289.5 eV is in line with other literature reports of N–C=O functionality in amide containing polymers.[56,57] Following irradiation the presence of the N–C=O group is still confirmed due to the presence of a peak with binding energy of 287.7 eV and C–N peak at 285.8 eV. Thus, it can be stated that the PEI-ZnTPP polymer is still present on the surface of the TiO_2 nanocomposites following 4 hours of irradiation under photocatalytic conditions. However, after 4 hours the intensity of two peaks with binding energies at 286.9, and 289.1 eV have increased relative to that of the amide N–C=O

signal. The binding energies of these two peaks are consistent with those of C=O and O–C=O functionalities, indicating degradation of the amide linkage to the carboxylic acid starting material.[58] Over the course of the experiments, the XPS studies indicates degradation of the nanocomposites occurs, and is reflected in the decrease in PHE rate of the system from 47 000 μmol g^{-1} h^{-1} after 1 hour of irradiation to 34 675 μmol g^{-1} h^{-1} after 4 h, and further to 24 600 μmol g^{-1} h^{-1} after 24 hours.

Electrochemistry

Hydrogen-producing photocatalytic assemblies based on the dye-sensitisation of TiO_2 depend on the injection of an electron from the photoexcited state of the dye to the conduction band of the semiconductor, in tandem with the regeneration of the ground-state dye through electron transfer from the SED.[59] To confirm the feasibility of these critical charge-transfer steps, CV measurements were conducted to obtain values for the frontier orbital energies of the PEI-ZnTPP polymer. Solution-phase voltammograms are presented in Fig. 6 for the polymer and molecular ZnTPP, recorded in the oxidative region of potential. In both cases two quasi-reversible redox waves are apparent in accordance with previous studies on ZnTPP.[23,60] These correspond to the ring centred radical cation, $[ZnTPP]^+$ and dication species, $[ZnTPP]^{2+}$, since for ZnTPP it is long established that no oxidation of the metal centre occurs.[61] In close agreement with the literature,[62] the first oxidation of ZnTPP was noted at a half-wave potential of $E_{ox_1} = 0.382$ V, while dication formation prevailed at $E_{ox_2} = 0.705$ V. For the PEI-ZnTPP polymer, small anodic shifts were apparent to values of $E_{ox_1} = 0.402$ V, and $E_{ox_2} = 0.725$ V. Following the common approach of identifying the first oxidation potential of a species with its HOMO level,[63,64] this implies a small stabilisation of this energy level upon ZnTPP incorporation into the PEI polymer. This observation is consistent with the amide linkage within the polymer, which consists of direct bonding of an electron-withdrawing carbonyl group to the porphyrin moiety.

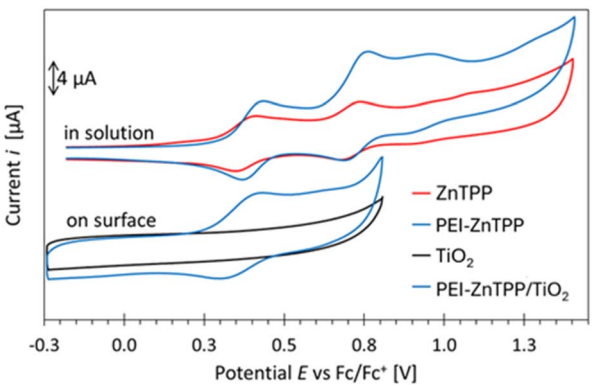

Fig. 6 Cyclic voltammograms of (upper) solution phase molecular ZnTPP and PEI-ZnTPP measured at a glassy carbon electrode, and (lower) TiO_2 and PEI-ZnTPP sensitised TiO_2 on FTO glass electrodes. The supporting electrolyte was 0.1 M tetrabutylammonium hexafluorophosphate/acetonitrile and all scans were recorded with an initial direction of increasing potential, at 100 $mV.s^{-1}$.

Since the photocatalytic system depends on adsorption of the polymer onto the semiconductor particles, voltammetry measurements were also conducted on TiO_2 electrodes sensitised by PEI-ZnTPP (Fig. 6). This surface immobilised CV is similar in profile to those previously reported for TiO_2 films functionalised by other ZnTPP-based dyes, with the initial quasi-reversible, redox wave remaining apparent, while the more positive wave was suppressed.[65] In further agreement with the literature on zinc porphyrins,[66,67] TiO_2 adsorption induces only a moderate shift in the formal potential for radical cation formation – in this case a cathodic shift to $E_{ox_1} = 0.365$ V.

A Rehm–Weller type thermodynamic analysis was conducted, as outlined in detail in section S4.[11] Summarising briefly, the energy gap, $E_{0,0}$, between the ground state and the relevant excited state vibrational level can be graphically extracted from the higher energy end of the PEI-ZnTPP phosphorescence spectrum (Fig. S17), leading to a value of $E_{0,0} = 1.64$ eV. The excited state oxidation potential E^*_{OX} can be estimated by subtracting $E_{0,0}$ from E_{ox_1} for the TiO_2 immobilised polymer, thereby yielding $E^*_{OX} = -1.28$ V. Converting this potential to an energy value relative to the vacuum level, gives an excited state energy E^* of −3.5 eV for PEI-ZnTPP. This lies above the conduction band edge of TiO_2, which was determined (from Mott–Schottky plots, Fig. S23) as approximately −4.4 eV under the conditions of our photocatalytic experiments, suggesting the favourability of electronic injection to the semiconductor particles from the excited state of the porphyrin-functionalised polymer. Furthermore, the energy associated with ascorbic acid oxidation (approximately −4.9 eV),[68] exceeds that of the PEI-ZnTPP HOMO level (≈ −5.2 eV, by conversion of E_{ox_1} to the vacuum scale), thereby permitting electron transfer from the SED to the polymer to sustain the catalytic cycle. Mott–Schottky plots also revealed that sensitisation of TiO_2 with PEI-ZnTPP and decoration with platinum nanoparticles has negligible effect on the energy of the conduction band edge. To obtain further insight into the charge transfer processes occurring during photocatalysis, photoanodes were fabricated by depositing films of the TiO_2 onto FTO glass slides with subsequent sensitisation by immersion in solutions of either ZnTPP or the PEI-ZnTPP polymer. An obvious green-to-yellow coloured staining of the TiO_2 film was observed in the case of the polymer, while no obvious colour change was noted for the molecular ZnTPP, indicating that surface adsorption may not have taken place in that case. The photocurrent response of these electrodes, under identical conditions of irradiation to the photocatalysis experiments, are presented in Fig. 7a. It is apparent that the PEI-ZnTPP functionalised photoanode delivers a photocurrent of approximately twice the magnitude of TiO_2, suggesting that the polymer effectively facilitates visible-light driven charge separation and electronic injection into the conduction band of the TiO_2. The electrode treated with ZnTPP delivers an almost identical response to pristine TiO_2, strongly suggesting that sensitisation is not possible for the molecular porphyrin. This observation agrees with the photocatalytic results, where it was noted that addition of ZnTPP to Pt/TiO_2 does not significantly enhance the photocatalytic hydrogen evolution activity compared to Pt/TiO_2 on its own.

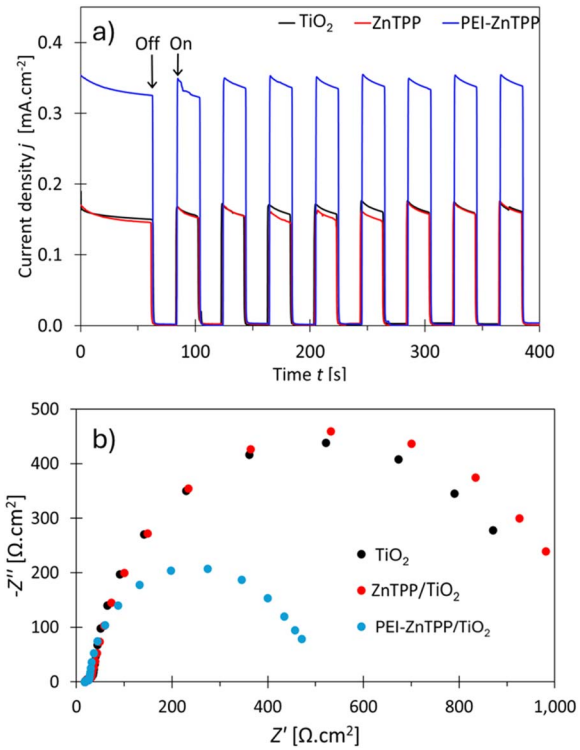

Fig. 7 (a) Photocurrent response plot of TiO_2 and TiO_2 sensitised electrodes measured at 0.1 V (Ag/AgCl) and (b) Nyquist plots of these electrodes measured at −0.24 V (Ag/AgCl). Identical irradiation conditions were used as for the photocatalysis. The electrolyte was 0.5 M Na_2SO_4 with ascorbic acid added at 2 g L^{-1}.

Electrochemical impedance spectroscopy (EIS) measurements were also performed on these photoelectrodes with the results obtained at −0.24 V (*vs.* Ag/AgCl) depicted in the Nyquist plot format in Fig. 7b. The impedance response of photosensitised TiO_2 films is commonly rationalised in terms of the so-called diffusion-recombination model developed by Bisquert and co-workers.[69,70] According to this approach, the mid-to-low range frequency response (10 s of kHz–mHz) of a TiO_2 photoelectrode may be driven by both the electron transport resistance (R_T) through the semiconducting oxide, and the charge transfer resistance (R_{CT}) at the sensitised oxide/electrolyte solution interface, with the relative influence of each depending on the applied potential. In particular, it has been shown that under similar pH and potential conditions to the data of Fig. 7b, the mid-to-low frequency Nyquist semicircle is characteristic of R_{CT}, with the arc profile becoming increasingly deformed as the potential is altered in the positive direction and R_T begins to predominate.[71] Accordingly, the diameter of the semicircular features of Fig. 7b can be regarding as being proportional to R_{CT}. A significantly lower resistance to interfacial charge transfer is evident for the PEI-ZnTPP sensitised film compared to TiO_2, or the film treated with ZnTPP. The combination of the enhanced photocurrent response and this EIS data suggest that the adsorbed PEI-ZnTPP improves visible light harvesting efficiency while enhancing surface charge transfer kinetics thereby leading to its superior photocatalytic activity.

Conclusions

In summary, hydrogen was generated using a nanocomposite mixture composed of PEI-ZnTPP polymer/TiO_2/Pt/AA, with visible light sensitisation. The PEI-ZnTPP polymer maintained the broad absorption in the visible region of the EM spectrum associated with the ZnTPP PS units, a long-lived triplet state lifetime (197 μs) at lower concentrations, and a biexponential signal with lifetimes of 29 μs and 146 μs attributed to the formation of different porphyrin microenvironments at the higher sample concentrations. Notably, a PHE rate of 34 675 μmol H_2 g^{-1} h^{-1} was obtained which is one of the highest rates for photosensitising polymers chemisorbed onto TiO_2. XPS analysis indicated that the prepared nanocomposites did not fully degrade over the PHE experiment. The PEI-ZnTPP polymer demonstrated that the incorporation of PSs such as porphyrins into polymers provides an effective approach to harnessing solar energy for hydrogen generation, with the electrochemical measurements verifying the favourablity of electron transfer from the excited state of the PEI-ZnTPP polymer into the conduction band of TiO_2 efficiently fuelling photocatalysis in the visible region of the EM spectrum, where ZnTPP alone showed significantly reduced activity. This was further supported by the enhancement of the photocurrent response of the TiO_2 photoelectrodes when sensitised by PEI-ZnTPP compared to molecular ZnTPP, while EIS measurements also suggested more facile charge transfer at the solution/composite interface in the presence of the polymer.

Experimental

Synthesis

All chemicals and solvents were supplied by Aldrich Chemicals Co. Scientific, and anhydrous solvents containing sure/seal were used under nitrogen. NMR spectra were recorded on a Bruker 600 MHz spectrometer and were referenced to the deuterated solvent peak as an internal reference. FT-IR spectra were obtained at room temperature using the Thermo Scientific Nicolet iS5 IR-ATR instrument and Omnic Spectra software. Gel permeation chromatography (GPC) was used to determine the dispersities (ĐM) and molecular weights of synthesized polymers. GPC was conducted in THF using a PSS SecCurity2 system equipped with GPC precolumn PSS SDV analytical in THF, 50 × 8 mm, 5 μm columns in series and a differential refractive index (RI) detector at a flow rate of 1.0 mL min^{-1}. The systems were calibrated against Varian Polymer Laboratories Easi-Vial linear poly(styrene) (PS) standards respectively and analysed by the software package WinGPC 8.40.

Synthesis of methyl mono-(*p*-carboxy)-tetraphenylporphyrin (Me-pcTPP). Me-pcTPP was prepared according to Lindsey's method for porphyrin synthesis. 3 Methyl 4-formylbenzoate (0.411 g, 2.5 mmol) was dissolved in dry CH_2Cl_2 (100 mL), where benzaldehyde (0.795 mL, 7.5 mmol), pyrrole (0.695 mL, 10 mmol), and ground sodium chloride (0.0585 g, 1.00 mmol) were added to. The solution was degassed with a stream of nitrogen under constant stirring at room temperature for 10 min. Boron trifluoride etherate (247 μL, 2.00 mmol) was added and the reaction mixture was stirred for another 60 min until methyl 4-formylbenzoate no longer was evident by TLC analysis. 2,3-

Dichloro-5,6-dicyano-1,4-benzoquinone (DDQ) (1.70 g, 7.5 mmol) was added, and the reaction was let continue for an hour. Triethylamine (1.00 mL) was added to the reaction mixture and the solvent was reduced *in vacuo*. The crude mixture was filtered over a short column of silica eluting with DCM followed by purification on silica eluting with DCM: hexane, 1 : 1. Methyl mono-(*p*-carboxy)-tetraphenylporphyrin (Me-pcTPP) 1 was isolated from the second purple band on silica column and gave deep purple crystals in 19% yield (0.315 g, 0.467 mmol). ^{1}H NMR ($CDCl_3$): 8.76–8.84 (m, 8H), 8.40 (d, $J = 7.9$ Hz, 2H), 8.28 (d, $J = 7.9$ Hz, 2H), 8.17–8.19 (m, 6H), 7.69–7.75 (m, 9H), 4.11 (s, 3H), −2.79 (s, 2H). 13C NMR (CDCl3): 166.3, 146.0, 141.0, 140.9, 133.5, 128.5, 126.8, 125.6, 119.5, 117.4, 51.4.

Synthesis of methyl mono-(*p*-carboxy)-tetraphenyl Zinc(II) porphyrin Zn(II) (Zn-Me-pcTPP). Free base porphyrin 1 (200 mg, 0.31 mmol) and zinc acetate dihydrate (0.680 g, 3.10 mmol) were stirred overnight in 60 mL of CH_2Cl_2/MeOH (7 : 3) at 40 °C. The solution was then washed with water (3 × 20 mL), dried over $MgSO_4$, and evaporated to dryness. The residue was taken up with the minimum amount of CH_2Cl_2 (5 mL) and precipitated by the addition of hexane (20 mL) to give 2 as a purple powder (205 mg, 100%). ^{1}H NMR ($CDCl_3$): d 8.78–8.86 (m, 8H), 8.40 (d, J = 7.9 Hz, 2H), 8.25 (d, J 13C NMR ($CDCl_3$): 167.4, 150.2, 149.4, 143.1, 134.5, 132.0, 131.8, 131.2, 129.1, 127.6, 126.4, 121.0, 52.3.

Synthesis of zinc(II) 4-(10,15,20-triphenylporphyrin-5-yl) benzoic acid, Zn(II) (Zn–COOH-TPP). To a solution of methyl mono-(*p*-carboxy)-tetraphenyl zinc(II) porphyrin Zn(II) (Zn–Me-pcTPP), 2 (220 mg, 0.311 mmol) in a THF/H_2O (4 : 1) mixture (8 mL) was added lithium hydroxide monohydrate (3.11 mmol, 0.075 g). The mixture was stirred at 0 °C for 12 h. The reaction mixture was divided between CH_2Cl_2 and 10% citric acid. The organic phase was washed with water, dried over $MgSO_4$ and evaporated to dryness. Subsequently, the product was precipitated with CH_2Cl_2/hexane to quantitatively give Zn–COOH-TPP as a purple powder (230 mg, 100%). ^{1}H NMR (d_6-DMSO): d 8.80–8.83 (m, 8H), 8.40 (d, $J = 8.0$ Hz, 2H), 8.34 (d, $J = 8.0$ Hz, 2H), 8.20–8.22 (m, 6H), 7.80–7.84 (m, 9H). ^{13}C NMR (d_6-DMSO): 168.0, 149.8, 149.3, 147.8, 143.1, 134.8, 134.6, 132.3, 131.8, 130.3, 127.9, 127.0, 121.1.

Synthesis of PEI-ZnTPP. Zn-COOH-TPP (0.28 mmol, 0.194 g) was suspended in dry CH_2Cl_2 (20 mL), and oxalyl chloride (2.8 mmol, 240 μL) was added followed by two drops of N,N′-dimethylformamide (as catalyst). The mixture was stirred at 25 °C for 10 h. The solvent was removed under reduced pressure and traces of oxalyl chloride were removed by the addition and subsequent evaporation of CH_2Cl_2 (2 × 3 mL). The residue was dissolved in dry THF (10 mL) and added to an ice-cold solution of polyethylenimine, branched (PEI) (0.028 mmol, 0.022 g) and triethylamine (1.4 mmol, 196 μL) in dry THF (10 mL). The mixture was stirred at 25 °C for another 8 h, concentrated under reduced pressure and the residue was partitioned between CH_2Cl_2 (50 mL) and water (50 mL). The organic extract was washed with $NaHCO_3$ 1% (2 × 50 mL) and water (2 × 50 mL) and dried over $MgSO_4$. The solvent was removed under reduced pressure to give the final product (yield: 94 mg, 83%). ^{1}H NMR ($CDCl_3$): 9.15–9.19 (m, 8H), 8.44–8.50 (m, 8H), 7.75–8.02 (m, 11H), 0.26–3.38 (m, 94H). ^{13}C NMR ($CDCl_3$): 170.4, 161.1, 150.4, 149.1, 148.7, 143.5, 141.9, 134.7, 133.4, 131.0, 130.9, 127.1, 126.3, 125.4, 124.4, 120.1, 119.9, 118.5, 67.4, 64.9, 52.3, 38.8, 35.3, 34.2, 33.1, 30.8, 30.1, 29.2, 28.6, 28.3, 26.6, 23.0, 21.6, 21.0, 20.1, 13.0. MW = 7164 g mol^{-1}, ĐM = 1.04 (RI detection, THF GPC).

Mass spectrometry

Mass spectrometry was conducted using a Waters LCT Premiere XE mass spectrometer. Electron spray ionisation (ESI) (positive mode, Na^+) and a time of flight (TOF) mass analyser were employed. The sample was dissolved in methanol.

Photophysical measurements

All photophysical characterisation was carried out using spectrophotometric grade solvents obtained from Thermofischer Scientific, without further purification. Steady state UV-vis and emission spectroscopy were collected in a 10 mm pathlength quartz cuvette at room temperature (295 K), using a Horiba DUETTATM absorbance and fluorescence spectrometer using EZSpec Software. For samples analysed on glass, 50 μL of a 2 mg ml^{-1} solution of PEI-ZnTPP dissolved in CH_2Cl_2 was drop cast onto a glass slide to prepare films which were directly analysed in the spectrometer.

Singlet oxygen quantum yield determination. Singlet oxygen quantum yields were determined *via* phosphorescence recorded at 1270 nm using a 512-element InGaAs diode array detector (Andor indus-InGaAs) coupled to a shamrock163 spectrograph (Andor Technology) *via* a round-to-line bundle of fibres (3, 105 micron diameter), with the sample held in a Thorlabs cuvette holder (CVH100/M^{-1}) with long pass filter to reject excitation light and scatter, and with excitation at 90o. All samples were prepared in aerated toluene to an absorbance of 0.3 a.u. at λex (405 nm fibre optic cable Thorlabs). Singlet oxygen quantum yields were determined as detailed in Section S2.1 of the SI.

Fluorescence lifetimes. Fluorescence lifetimes and quantum yields were recorded using a FLS1000 photoluminescence spectrometer (Edinburgh Instruments). All samples were prepared to an absorbance of 0.3 a.u. at the wavelength of excitation using aerated toluene/THF in a 10 mm pathlength quartz cuvette. For determining fluorescence quantum yields, samples were irradiated using a Xe Arc Lamp in an integrating sphere with an excitation wavelength of 420 nm. Emission lifetimes were determined *via* time correlated single photon counting (TCSP), using a 375 nm picosecond pulsed diode laser. Lifetimes were fitted according to Section S2.2 of the SI.

Ns-transient absorption spectroscopy. Ns-TAS was performed using a LP980 transient absorption spectrometer (Edinburgh Instruments), using 355 nm laser excitation generated using a Quantel Q-Smart 450 pulsed laser. Samples were degassed *via* three freeze-pump-thaw cycles followed by open to liquid pump to remove any formed azeotropes, followed by headspace replacement using N_2 gas prior to experimentation. Transient absorption lifetimes were fitted as described in the SI Section S2.2.

Photocatalytic hydrogen evolution

All photocatalysis was performed using a G2V Optics SunbrickTM Large Area AAA LED Solar Simulator (λ_{ex} 400–900 nm) as a source of irradiation. All samples were degassed prior to irradiation *via* three freeze-pump-thaw cycles followed by replacement of the headspace of the photocatalysis vessel with N_2 gas. Hydrogen production was quantified *via* sampling of 1 ml portions of the headspace gas *via* gas chromatography employing a Shimadzu GC-210 with BID detector on a 5 Å molecular sieve column using He as a carrier gas, with oven temperature at 30 °C. Hydrogen production was determined *via* reference to a 1000 ppm H_2 gas standard (CalgazTM). All PHE parameters were calculated as described in Section S3.1.

Pt^0 was photodeposited onto TiO_2 nanoparticles according to modified literature procedures.[72,73] To a 18 ml Schlenk tube 2.67 ml of a 1 mg ml^{-1} $H_2PtCl_6 \cdot 6H_2O$ solution (equivalent to 1 mg Pt^0 content) was added followed by an equal volume of MeOH. 100 mg of TiO_2 anatase, nano powder, < 25 nm particle size was added. The mixture was purged with N_2 for 30 minutes, followed by sonication for 15 minutes to create an even particle distribution. The solution was then irradiated using a s olar simulator (λ_{ex} 400–900 nm) for 4 hours. A colour change from an orange solution to grey was observed corresponding to reduction of Pt^{IV} to Pt^0. The product was collected *via* centrifugation, and dried under vacuum at 70 °C for 2 hours to yield 76 mg of 1 wt% Pt on TiO_2 powder.

Photocatalysis samples were prepared as follows: the desired weighting of PEI-ZnTPP was dissolved using 1 ml THF in an 18 ml Schlenk tube, fitted with magnetic stir bar. To this 5 mg of the previously prepared 1 wt% Pt on TiO_2 powder was added, and the mixture was suspended *via* sonication for 15 minutes. The mixture was then stirred for 15 minutes, and solvent was evaporated. To the PEI-ZnTPP/Pt^0/TiO_2 mixture, 3 ml sacrificial agent solution [0.8 M ascorbic acid (adjusted to pH of 5-6 using 0.2 M NaOH), 20% triethanolamine (adjusted to a pH of 7 using HCl) or 20% MeOH] was added. The Schlenk tube was sealed using a rubber septum, and the sample was degassed. Once degassed, the sample was sonicated for 15 minutes to create an even dispersion, followed by irradiation using the solar simulator with constant stirring.

X-ray photoelectron spectroscopy

XPS analysis was carried out on a Kratos AXIS ULTRA spectrometer using a monochromatic Al Kα source. The area of analysis was approximately 1 mm^2. C 1s line at 284.8 eV was used as a charge reference. Construction and peak fitting of synthetic peaks in narrow region spectra used a Shirely type background and the synthetic peaks were of a mixed Gaussian-Lorenzian type. Relative sensitivity factors used are from CasaXPS library containing Scofield cross-sections.

Electrochemistry

The cyclic voltammetry measurements were performed at room temperature using a CHI 750C electrochemical workstation. The supporting electrolyte was 0.1 M tetrabutylammonium hexafluorophosphate ($TBAPF_6$-Sigma-Aldrich ≥99.0%) in dry acetonitrile. For molecular ZnTPP a 1 mM test solution was prepared in this background electrolyte. In the case of the PEI-ZnTPP polymer, the test solution was prepared to approximately 1 mM with respect to porphyrin centres on the basis of the number average molecular mass, M_n. The electrolyte solutions were deoxygenated by purging with nitrogen gas for a least 20 minutes, and a blanket of this inert gas was maintained above the solution during the measurements.

The surface CVs were measured in 1 M $TBAPF_6$/acetonitrile using pristine and sensitised TiO_2 electrodes. These were prepared on cleaned fluorine-doped tin oxide (FTO) glass substrates following a adaption of the method outlined by Nawawi *et al.*[74] In brief, the TiO_2 powder (100 mg) was ultrasonically dispersed in deionised water (750 µl) to which was added 15 µl of an 8 w/v polyethylene glycol (PEG, av. $M_w = 8000$) aqueous solution. A 1 × 1 cm area was defined on the FTO glass surface using kapton tape, into which TiO_2 dispersion (20 µl) was pipetted and spread with a glass rod. The substrate was then dried on a hot plate at 50 °C for 10 minutes, before progressively ramping the temperature to 500 °C where it was maintained for 30 minutes, prior to allowing natural cooling. Sensitisation was attempted by immersing the TiO_2/FTO substrates, while still warm (80 °C), in ZnTPP (0.2 mM) or PEI-ZnTPP (~0.2 mM in porphyrin centres) solutions in a 1 : 1 v/v methanol/THF solvent mixture. The sensitisation vials were maintained in the dark for 12 hours and the substrates were then rinsed thoroughly with methanol/THF. The approximate dry loading of TiO_2 is of the order of 2.5 $mg.cm^{-2}$.

A three-electrode cell setup was utilised with a glassy carbon disk working electrode for the solution phase CV measurements, and a platinum gauze counter electrode. The potential was measured against an Ag^+ non-aqueous reference electrode, consisting of a silver wire immersed in a 0.01 M $AgNO_3$/0.1 M $TBAPF_6$/acetonitrile solution, and separated from the rest of the cell by a porous frit. The reference electrode was calibrated against ferrocene (a 1 mM solution in 0.1 M $TBAPF_6$/acetonitrile) after each measurement, and all potentials are quoted relative to the ferrocenium/ferrocene (Fc^+/Fc) couple. The voltammograms were recorded at a scan rate of 100 $mV.s^{-1}$. The formal potentials of the redox reactions were determined by taking the half-wave potential, $E_{1/2}$, given that $E_{1/2} = (E_a + E_c)/2$, where E_a and E_c are the anodic and cathodic peak potentials, respectively.

Electrochemical impedance spectroscopy (EIS), Mott–Schottky, and photocurrent measurements were performed with the sensitised-TiO_2/FTO substrates as working electrodes, using a BioLogic VSP potentiostat under conditions of simulated solar irradiation. The reference electrode for these aqueous electrochemical measurements was Ag/AgCl (3M KCl), with a platinum gauze counter electrode. The Mott–Schottky experiments were performed in a 0.5 M sodium sulfate solution (measured pH 6.6), while ascorbic acid (2 g L^{-1}) was added a similar solution (giving a pH of 3.4) for the EIS and photocurrent measurements. The EIS data was collected over a frequency range from 200 kHz to 40 mHz, with an ac perturbation of 5 mV amplitude.

Conflicts of interest

There are no conflicts of interest to declare.

Data availability

All experimental data supporting the findings of this study are available within the article and its supplementary information (SI) file. Raw spectroscopic data generated during the study are available from the corresponding author upon reasonable request.

Supplementary information: NMR, FTIR, additional photophysical measurements, further details on the thermodynamic analysis and Mott–Schottky data. See DOI: https://doi.org/10.1039/d5se01588j.

Acknowledgements

This work was funded by the Sustainable Energy Authority of Ireland (SEAI) under grants 22/RDD/890 and 24/RDD/1186 and Research Ireland (Awards 19/FFP/6882).

Notes and references

1 L. Wang, L. Wang, Y. Li and J. Wang, *Decis. Anal. J.*, 2023, **7**, 100237.
2 The World Meteorological Organization (WMO), *State of the Global Climate 2024*, WMO, Geneva, 2025.
3 M. M. Hossain Bhuiyan and Z. Siddique, *Int. J. Hydrogen Energy*, 2025, **102**, 1026–1044.
4 N. I. Badea, *Energies*, 2021, **14**, 5783.
5 A. Wawrzyńczak and A. Feliczak-Guzik, *Coatings*, 2024, **14**, 366.
6 A. FUJISHIMA and K. HONDA, *Nature*, 1972, **238**, 37–38.
7 P. D. Tran, L. H. Wong, J. Barber and J. S. C. Loo, *Energy Environ. Sci.*, 2012, **5**, 5902–5918.
8 L. G. de Araujo and D. Farrusseng, *New J. Chem.*, 2025, **49**, 6888–6913.
9 L. R. Milgrom, *The Colours of Life. An Introduction to the Chemistry of Porphyrins and Related Compounds*, Oxford University Press, Oxford, 1st edn, 1997.
10 M. Gouterman, *J. Mol. Spectrosc.*, 1961, **6**, 138–163.
11 J. S. O'Neill, L. Kearney, M. P. Brandon and M. T. Pryce, *Coord. Chem. Rev.*, 2022, **467**, 214599.
12 Y. Kuramochi and A. Satake, *Catalysts*, 2023, **13**, 282.
13 A. Akbar, S. Khan, T. Chatterjee and M. Ghosh, *J. Photochem. Photobiol. B Biol.*, 2023, **248**, 112796.
14 H. Huang, W. Song, J. Rieffel and J. F. Lovell, *Front. Phys.*, 2015, **3**, 23.
15 D. R. Bitsos, A. Salepis, E. Orfanos, A. G. Coutsolelos, R. I. Kosheleva, A. C. Mitropoulos and K. Ladomenou, *Inorganics*, 2025, **13**, 121.
16 Y. Yuan, H. Lu, Z. Ji, J. Zhong, M. Ding, D. Chen, Y. Li, W. Tu, D. Cao, Z. Yu and Z. Zou, *Chem. Eng. J.*, 2015, **275**, 8–16.
17 E. Koposova, X. Liu, A. Pendin, B. Thiele, G. Shumilova, Y. Ermolenko, A. Offenhäusser and Y. Mourzina, *J. Phys. Chem. C*, 2016, **120**, 13873–13890.
18 X. Feng, Z. Liu, L. Qin, S.-Z. Kang and X. Li, *Phys. Chem. Chem. Phys.*, 2020, **22**, 13528–13535.
19 T. Zheng, A. Li, H. Tu, L. Pan, S. Sasaki and X.-F. Wang, *Mater. Today Energy*, 2024, **44**, 101631.
20 V. Nikolaou, G. Charalambidis, G. Landrou, E. Nikoloudakis, A. Planchat, R. Tsalameni, K. Junghans, A. Kahnt, F. Odobel and A. G. Coutsolelos, *ACS Appl. Energy Mater.*, 2021, **4**, 10042–10049.
21 V. Nikolaou, E. Agapaki, E. Nikoloudakis, K. Achilleos, K. Ladomenou, G. Charalambidis, E. Triantafyllou and A. G. Coutsolelos, *Chem. Commun.*, 2023, **59**, 11256–11259.
22 F. Li, K. Yang, J. S. Tyhonas, K. A. MacCrum and J. S. Lindsey, *Tetrahedron*, 1997, **53**, 12339–12360.
23 J. Rochford, S. Botchway, J. J. McGarvey, A. D. Rooney and M. T. Pryce, *J. Phys. Chem. A*, 2008, **112**, 11611–11618.
24 M. Vasilopoulou, A. M. Douvas, D. G. Georgiadou, V. Constantoudis, D. Davazoglou, S. Kennou, L. C. Palilis, D. Daphnomili, A. G. Coutsolelos and P. Argitis, *Nano Res.*, 2014, **7**, 679–693.
25 M. Vasilopoulou, D. G. Georgiadou, A. M. Douvas, A. Soultati, V. Constantoudis, D. Davazoglou, S. Gardelis, L. C. Palilis, M. Fakis, S. Kennou, T. Lazarides, A. G. Coutsolelos and P. Argitis, *J. Mater. Chem. A*, 2014, **2**, 182–192.
26 M. Zannotti, R. Giovannetti, B. Minofar, D. Řeha, L. Plačková, C. A. D'Amato, E. Rommozzi, H. V. Dudko, N. Kari and M. Minicucci, *Spectrochim. Acta, Part A*, 2018, **193**, 235–248.
27 M. Ghosh, A. K. Mora, S. Nath, A. K. Chandra, A. Hajra and S. Sinha, *Spectrochim. Acta, Part A*, 2013, **116**, 466–472.
28 M. Taniguchi, J. S. Lindsey, D. F. Bocian and D. Holten, *J. Photochem. Photobiol., C*, 2021, **46**, 100401.
29 M. Gouterman and G.-E. Khalil, *J. Mol. Spectrosc.*, 1974, **53**, 88–100.
30 R. T. Kuznetsova, E. G. Ermolina, R. M. Gadirov, G. V. Mayer, P. A. Stuzhin, I. P. Kalashnikova and Y. V. Korovin, *J. Porphyrins Phthalocyanines*, 2008, **12**, 1173–1181.
31 L. Tabrizi, R. McGarry, K. Turzanska, L. Varvarezos, M. Fallon, R. Brannigan, J. T. Costello, D. Fitzgerald-Hughes and M. T. Pryce, *Biomacromolecules*, 2024, **25**, 7736–7749.
32 C. Brady, S. E. J. Bell, C. Parsons, S. P. Gorman, D. S. Jones and C. P. McCoy, *J. Phys. Chem. B*, 2007, **111**, 527–534.
33 Ö. A. Bozdemir, D. D. Gultekin and A. Harriman, *J. Phys. Chem. A*, 2020, **124**, 10736–10747.
34 G. G. Parra, D. S. Correa, E. Silveira-Alves, L. M. Almeida, M. A. R. Souza, L. De Boni, L. Misoguti, C. R. Mendonça, S. C. Zílio, N. M. Barbosa Neto, I. E. Borissevitch and P. J. Gonçalves, *Spectrochim. Acta, Part A*, 2021, **261**, 120063.
35 M. Orfanopoulos, *Photochem. Photobiol.*, 2021, **97**, 1182–1218.
36 O. Suryani, Y. Higashino, H. Sato and Y. Kubo, *ACS Appl. Energy Mater.*, 2019, **2**, 448–458.
37 G. Mukherjee, J. Thote, H. B. Aiyappa, S. Kandambeth, S. Banerjee, K. Vanka and R. Banerjee, *Chem. Commun.*, 2017, **53**, 4461–4464.

38 M. M. Almutairi, E. E. Ebraheim, M. S. Mahmoud, M. S. Atrees, M. E. M. Ali and Y. M. Khawassek, *Egypt. J. Chem.*, 2019, **62**, 1649–1658.
39 A. Kathiravan and R. Renganathan, *J. Colloid Interface Sci.*, 2009, **331**, 401–407.
40 X. Liu, H. Lai, J. Li, G. Peng, Z. Yi, R. Zeng, M. Wang and Z. Liu, *Int. J. Hydrogen Energy*, 2019, **44**, 4698–4706.
41 C. N. Matindi, S. Kadanyo, G. Liu, M. Hu, Y. Hu, Z. Cui, X. Ma, F. Yan, B. He and J. Li, *J. Water Proc. Eng.*, 2022, **49**, 102982.
42 K. Turgut, M. Özdemir, G. Yıldız, B. Yalçın, S. Koyuncu, B. Köksoy and İ. Hatay Patır, *Int. J. Hydrogen Energy*, 2025, **158**, 150105.
43 J.-Y. Mao, S.-X. Ye, Y. Yang, C.-J. Lu, X.-L. Sun, H. Xue and W.-M. Wan, *Polym. Chem.*, 2025, **16**, 3432–3442.
44 T. Mauerer, J. Hungenberg, M. Thelakkat and R. Marschall, *J. Polym. Sci.*, 2025, **63**, 4684–4697.
45 H. Gong, Y. Xing, J. Li and S. Liu, *Molecules*, 2024, **29**, 1103.
46 S. Palenzuela-Rebella, T. Naranjo, M. Gomez-Mendoza, M. Barawi, M. Liras and V. A. de la Peña O'Shea, *Adv. Funct. Mater.*, 2024, **34**, 2403778.
47 R. Isci, H. Bildirir, D. Gunturkun, M. Gomez-Mendoza, M. Liras, V. A. de la Peña O'Shea and T. Ozturk, *J. Mater. Chem. C*, 2024, **12**, 16108–16119.
48 X. Zhao, X. Zhang, Y. Liang, Z. Hu and F. Huang, *Macromolecules*, 2021, **54**, 4902–4909.
49 Z. Chen, J. Wang, S. Zhang, Y. Zhang, J. Zhang, R. Li and T. Peng, *ACS Appl. Energy Mater.*, 2019, **2**, 5665–5676.
50 Z. Xu, X. Cui, Y. Li, Y. Li, Z. Si and Q. Duan, *Appl. Surf. Sci.*, 2023, **613**, 155966.
51 R. Chen, Y. Wang, Y. Ma, A. Mal, X.-Y. Gao, L. Gao, L. Qiao, X.-B. Li, L.-Z. Wu and C. Wang, *Nat. Commun.*, 2021, **12**, 1354.
52 M. Lv, X. Ren, R. Cao, Z. Chang, X. Chang, F. Bai and Y. Li, *Polymers*, 2022, **14**, 4893.
53 H. Liu, S. Chen, Y. Zhang, R. Li, J. Zhang and T. Peng, *Mater. Today Sustain.*, 2022, **19**, 100164.
54 J. Lee and W. Choi, *J. Phys. Chem. B*, 2005, **109**, 7399–7406.
55 M. V. Lebedeva, A. V. Ragutkin, A. P. Antropov and N. A. Yashtulov, *IOP Conf. Ser. Mater. Sci. Eng.*, 2020, **744**, 012007.
56 M. Kehrer, J. Duchoslav, A. Hinterreiter, M. Cobet, A. Mehic, T. Stehrer and D. Stifter, *Plasma Processes Polym.*, 2019, **16**, 1800160.
57 S. Wang, Y. Fan, Q. Wang, L. Yang, J. Shang, S. Qiu and W. Zhang, *J. Mater. Sci.*, 2018, **53**, 10835–10845.
58 K.-C. Chang, W.-F. Ji, M.-C. Lai, Y.-R. Hsiao, C.-H. Hsu, T.-L. Chuang, Y. Wei, J.-M. Yeh and W.-R. Liu, *Polym. Chem.*, 2014, **5**, 1049–1056.
59 L. Zani, M. Melchionna, T. Montini and P. Fornasiero, *J. Phys.: Energy*, 2021, **3**, 031001.
60 F. D'Souza, G. R. Deviprasad, M. E. Zandler, V. T. Hoang, A. Klykov, M. VanStipdonk, A. Perera, M. E. El-Khouly, M. Fujitsuka and O. Ito, *J. Phys. Chem. A*, 2002, **106**, 3243–3252.
61 A. Wolberg and J. Manassen, *J. Am. Chem. Soc.*, 1970, **92**, 2982–2991.
62 K. Aoki, T. Goshima, Y. Kozuka, Y. Kawamori, N. Ono, Y. Hisaeda, H. D. Takagi and M. Inamo, *Dalton Trans.*, 2009, 119–125.
63 R. E. M. Willems, C. H. L. Weijtens, X. de Vries, R. Coehoorn and R. A. J. Janssen, *Adv. Energy Mater.*, 2019, **9**, 1803677.
64 R. E. Aderne, B. G. A. L. Borges, H. C. Ávila, F. von Kieseritzky, J. Hellberg, M. Koehler, M. Cremona, L. S. Roman, C. M. Araujo, M. L. M. Rocco and C. F. N. Marchiori, *Mater. Adv.*, 2022, **3**, 1791–1803.
65 M. T. Brumbach, A. K. Boal and D. R. Wheeler, *Langmuir*, 2009, **25**, 10685–10690.
66 Q. Wang, W. M. Campbell, E. E. Bonfantani, K. W. Jolley, D. L. Officer, P. J. Walsh, K. Gordon, R. Humphry-Baker, M. K. Nazeeruddin and M. Grätzel, *J. Phys. Chem. B*, 2005, **109**, 15397–15409.
67 J. Rochford and E. Galoppini, *Langmuir*, 2008, **24**, 5366–5374.
68 M. Rueda, A. Aldaz and F. Sanchez-Burgos, *Electrochim. Acta*, 1978, **23**, 419–424.
69 A. Sacco, *Renew. Sustain. Energy Rev.*, 2017, **79**, 814–829.
70 A. R. C. Bredar, A. L. Chown, A. R. Burton and B. H. Farnum, *ACS Appl. Energy Mater.*, 2020, **3**, 66–98.
71 J. Bisquert, *J. Phys. Chem. B*, 2002, **106**, 325–333.
72 J. M. Herrmann, J. Disdier and P. Pichat, *J. Phys. Chem.*, 1986, **90**, 6028–6034.
73 A. Kubiak, M. V. Dozzi, M. Montalbano and M. Cegłowski, *Arab. J. Chem.*, 2024, **17**, 105846.
74 W. I. Nawawi, R. Zaharudin, M. A. Ishak, K. Ismail and A. Zuliahani, *Appl. Sci.*, 2017, **7**, 24.

